





OPEN

Corrosion mitigation characteristics of some novel organoselenium thiourea derivatives for acid pickling of C1018 steel via experimental and theoretical study

Hany M. Abd El-Lateef^{1,2}, Mai M. Khalaf^{1,2}, Mohamed Gouda¹, T. A. Yousef^{3,4}, Sayed H. Kenawy^{3,5}, Mortaga M. Abou-Krishna^{3,6}, Mohamed Alaasar^{7,8} & Saad Shaaban^{1,9}

Two organoselenium thiourea derivatives, 1-(4-(methylselanyl)phenyl)-3-phenylthiourea (DS036) and 1-(4-(benzylselanyl)phenyl)-3-phenylthiourea (DS038) were produced and categorized using FTIR and NMR (¹H and ¹³C). The effectiveness of the above two compounds as C-steel corrosion inhibitors in molar HCl was evaluated using the potentiodynamic polarization (PD) and electrochemical impedance spectroscopy (EIS) techniques. PD findings indicate that DS036 and DS038 have mixed-type features. EIS results show that growing their dose not only changes the polarization resistance of C-steel from 18.53 to 363.64 and 463.15 Ω cm² but also alters the double layer capacitance from 710.9 to 49.7 and 20.5 μF cm⁻² in the occurrence of 1.0 mM of DS036 and DS038, respectively. At a 1.0 mM dose, the organoselenium thiourea derivatives displayed the highest inhibition efficiency of 96.65% and 98.54%. The inhibitory molecule adsorption proceeded along the Langmuir isotherm on the steel substrate. The adsorption-free energy of the adsorption process was also intended and indicated a combined chemical and physical adsorption on the C-steel interface. FE-SEM studies support the adsorption and protective abilities of the OSe-based molecule inhibitor systems. In Silico calculations (DFT and MC simulations) explored the attraction between the studied organoselenium thiourea derivatives and corrosive solution anions on a Fe (110) surface. The obtained results show that these compounds can make a suitable preventing surface and control the corrosion rate.

Excellent mechanical qualities make carbon steel (C-steel) an essential material with a broad scope of uses in different areas including the marine and petroleum sectors¹. C-steels are easily corroded in acidic environments, principally in hydrochloric acid that is used for industrial pickling, acid descaling, cleaning, and oil well acidizing². The annual loss cost could be calculated to reach billions of dollars³. Although many strategies, including coating and deposition, were created to prevent metals from corroding⁴⁻⁷, the usage of corrosion inhibitors is still among the best and most efficient strategies^{8,9}. Corrosion inhibitors are distinguished by their

¹Department of Chemistry, College of Science, King Faisal University, 31982 Al-Hasa, Saudi Arabia. ²Department of Chemistry, Faculty of Science, Sohag University, Sohag 82524, Egypt. ³College of Science, Chemistry Department, Imam Mohammad Ibn Saud Islamic University (IMSIU), 11623 Riyadh, Kingdom of Saudi Arabia. ⁴Department of Toxic and Narcotic Drug, Forensic Medicine, Mansoura Laboratory, Medicolegal Organization, Ministry of Justice, Mansoura, Egypt. ⁵Refractories, Ceramics and Building Materials Department, National Research Centre, El-Buhouth St., Dokki, Giza 12622, Egypt. ⁶Department of Chemistry, South Valley University, Qena 83523, Egypt. ⁷Institute of Chemistry, Martin Luther University Halle-Wittenberg, Halle, Germany. ⁸Department of Chemistry, Faculty of Science, Cairo University, Giza, Egypt. ⁹Department of Chemistry, Faculty of Science, Mansoura University, Mansoura 35516, Egypt. ✉email: hmahmed@kfu.edu.sa; hany_shubra@science.sohag.edu.eg; sibrahim@kfu.edu.sa

strong capacity for adhesion to metallic surfaces. The corrosion rate is immediately reduced when the inhibitor is added in modest amounts since it quickly prevents corrosion¹⁰.

Due to their abundance in adsorption centers, such as hetero atoms (sulfur, oxygen, and nitrogen), organic molecules are frequently utilized as efficient corrosion inhibitors for mild steel in aqueous conditions. This makes the inhibitors cost-effective^{7,11,12}. The mutual contacts between the metal surface and the organic layer, which are controlled by an adsorption mechanism, can significantly slow down the rate of both anodic and cathodic corrosion reactions at the metal/solution interface^{13,14}. While electrochemical techniques like electrochemical impedance spectroscopy and potentiodynamic polarization can measure the rate of corrosion, theoretical simulations can measure the interactions between metals and inhibitors¹⁵.

Organoselenium (OSe) hybrids have recently gained much attention as a result of their diverse applications, particularly in material and medicinal chemistry^{16,17}. The selenium (Se) unprecedented characteristics and redox properties secured the potential biochemical and industrial applications of OSe agents¹⁸. The lower electronegativity and larger size of Se compared to its analogs sulfur, nitrogen, and phosphorous, are the main reasons for its higher polarizability and thus nucleophilicity¹⁷. Consequently, organoselenium (OSe) compounds are generally good nucleophiles and possess potential catalytic and chelating activities¹⁷. Unlike sulfur, Se is a semiconductor and showed photoconductive and photovoltaic properties it is therefore used extensively in material science and electronics, such as solar cells, sodium-ion batteries, photocells, and light meters¹⁷.

During the past decades, many corrosion inhibitors were developed and have shown considerable inhibition activities; however, they only function well at room temperature and at low acid concentrations^{8–10}. Therefore, inhibitors withstanding harsh conditions i.e., high temperature and concentrated acid (> 15 wt % HCl) are highly required in pipeline cleaning solutions and acidizing fluids, as well as in the petrochemical industries. Within this context, thioureas have shown potential application in retarding the corrosion of aluminum, copper, ferrous, zinc, and magnesium metals in different aggressive media by influencing the cathodic and anodic reactions. They acted as ideal adsorption sites in potential inhibitors owing to their ability to share free electrons with the metal template via their two nitrogen and sulfur atoms thus protecting the metals from acid corrosion by preventing the contact surface area available with hydrogen ions¹⁶. On the other hand, OSe compounds are considered better corrosion inhibitors than their organosulfur homologous owing to the Se greater ability to share its outer electrons with metals. Unfortunately, the anticorrosive efficacy of the OSe agents was seldom discussed and limited to a few examples in the literature. Recently, we reported different organoselenocyanates- (**I** and **II**) and diselenide-based (**III** and **IV**) water-soluble OSe compounds corrosion inhibitors for reinforced steel in the simulated concrete pore solution¹⁹. Moreover, we developed several OSe-tethered anthranilic acid hybrids (**V**, **VI**, and **VII**) as potential corrosion inhibitors for the J55 pipeline steel and 6061 aluminum alloy²⁰. Additionally, we have also reported OSe-based tetrazoles (**VIII**, and **IX**) as promising corrosion inhibitors for the J55 steel tubing samples during oil well acidizing (Fig. 1)²¹.

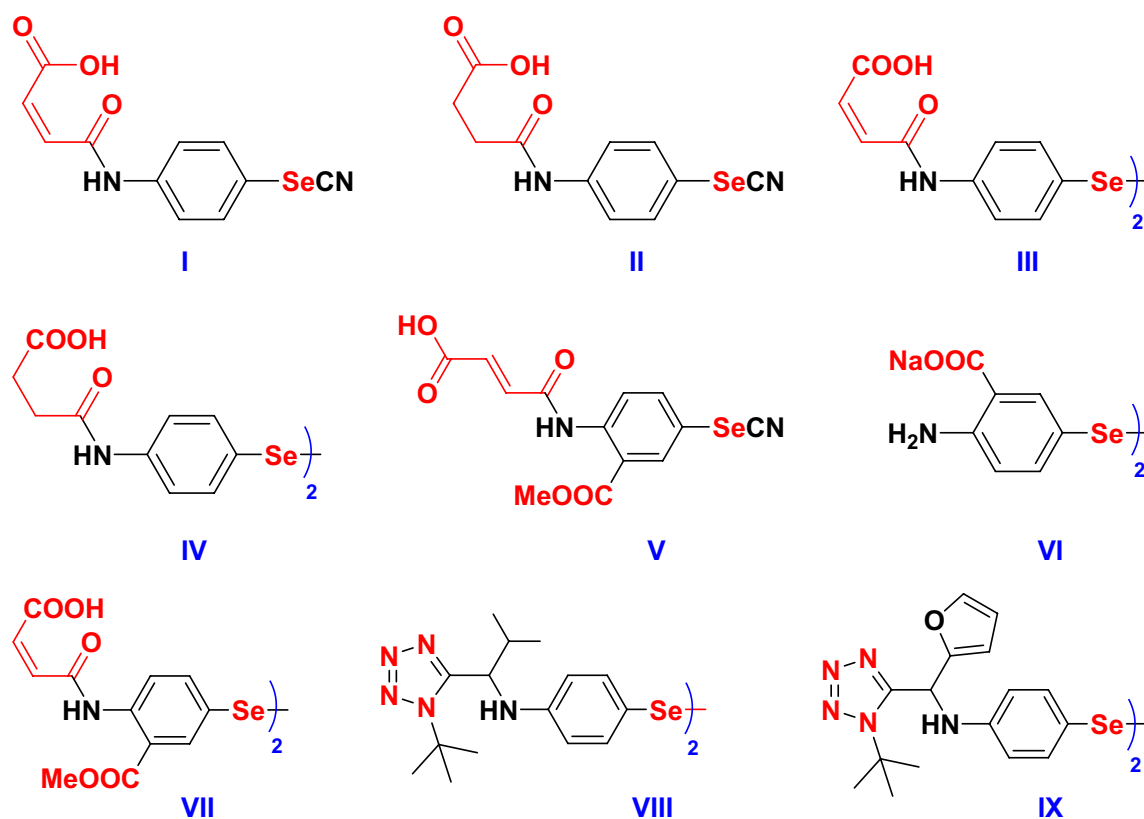


Figure 1. Organoselenium hybrids with promising corrosion inhibition properties.

It is therefore anticipated that a proper combination of thiourea and organoselenium compounds would enhance the overall corrosion inhibition activity. Accordingly, the present study focused on the preparation and structural investigation of organoselenium thiourea derivatives using a facile method, and spectroscopic methods (FTIR, ^1H NMR, and ^{13}C NMR). The study correspondingly involved the estimation of the synthesized OSe agents as inhibitors for C-steel corrosion in pickling solution using several electrochemical methods such as PDP and EIS. Furthermore, the molecular reactivity strictures on both the atomic and molecular levels were studied by means of DFT calculations to account for inhibitor–metal interactions, which is important to comprehend corrosion inhibition proficiency. The effectiveness of each inhibitor in relation to its orientation and structure, as well as the method by which an inhibitor adheres to metal surfaces, are thoroughly explained by the Monte Carlo simulations.

Experimental work

Materials, reagents, and methods. In this work, carbon steel with the following composition: P (0.046%), Si (0.35%), C (0.23%), Mn (1.42%), Cr (0.13%), Ni (0.034%), and Fe (rest) with an active area of $\approx 1\text{ cm}^2$ was used as the working electrode and scratched by various grades of emery papers (up to 1500 grade), degreased with acetone, rinsed with bidistilled H_2O , and dried with faint tissues. The experiments were complemented in molar HCl solution in the nonappearance and existence of various doses of the examined organoselenium thiourea compounds **DS036** and **DS038**. For each test, the component concentrations were ordered from 2×10^{-5} to $1.0 \times 10^{-3}\text{ M}$; a freshly discarded solution was used.

Melting points were recorded in degree centigrade using the Gallenkamp instrument. Spectra for the FTIR were recorded (KBr , $\nu\text{ cm}^{-1}$) at King Faisal University on Mattson 5000 FTIR Spectrophotometer. The ^1H NMR and the ^{13}C -NMR spectra were measured using Varian Spectrophotometer at 400 MHz and 500 MHz, employing the TMS internal reference and $\text{DMSO}-d_6$ as the solvents. The chemical shifts (δ) in parts per million were recorded with respect to the residual peak of solvents. Compounds 2–5 were synthesized according to our literature reports (see Fig. 2) (see detailed experimental procedures in the Supporting Materials)^{22–29}.

Synthesis and characterization. The OSe thiourea derivatives **DS036** and **DS038** were efficiently synthesized from readily available chemicals (e.g., aniline, phenyl isothiocyanate, SeO_2). All the reactions were straightforward and proceeded smoothly with classical and simple workups. The OSe thiourea derivatives **DS036** and **DS038** were obtained in moderate to high (57–89%) yields as well as in high purity as they recrystallized efficiently in ethanol without the need for sophisticated isolation using column chromatography. Furthermore, the **DS036** and **DS038** have different proton acceptor centers (e.g., nitrogen, sulfur, and Se) and this might be the reason for their good solubility in the HCl solution. Indeed, they are also readily soluble in different organic solvents such as acetone, DMF, and DMSO.

Interestingly, many organoselenium reactions were reported to proceed faster in water, and therefore the synthesis of **DS036** and **DS038** is worth further investigation under green conditions in the future once they are established as potential inhibitors.

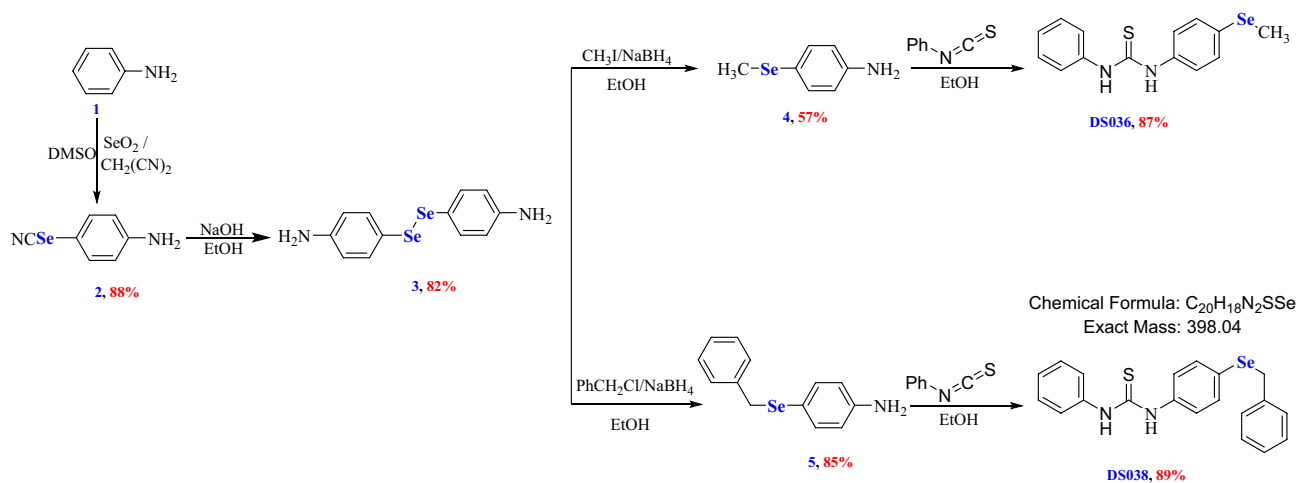


Figure 2. Synthesis of organoselenium compounds 2–5, **DS036** and **DS038**. (a) Selenocyanate 2 was obtained in 88% yield from aniline (2.5 mmol), $\text{CH}_2(\text{CN})_2$ (1.5 mmol), SeO_2 (3 mmol), and DMSO (5 mL); (b) Diselenide 3 was synthesized in 82% yield from selenocyanate 2 (0.5 mmol), NaOH (0.5 mmol), and ethanol (6 mL); (c) Selenide 4 was obtained in 57% yield from diselenide 3 (1 mmol), methyl iodide (2.2 mmol), and EtOH (20 mL); (d) Selenide 5 was obtained in 85% yield from diselenide 3 (1 mmol), benzyl chloride (2.2 mmol), and EtOH (20 mL); (e) Thiourea **DS036** was obtained in 87% yield from selenide 4 (1 mmol), phenyl isothiocyanate (1.2 mmol), and EtOH (10 mL); (f) Thiourea **DS038** was obtained in 89% yield from selenide 5 (1 mmol), phenyl isothiocyanate (1.2 mmol), and EtOH (10 mL).

General procedure for the synthesis of OSe thiourea derivatives DS036 and DS038. To a solution of organic selenide **4** or **5** (1 mmol) in (10 ml) ethanol, phenyl isothiocyanate (1.2 mmol) was added, and the mixture was refluxed for 6 h. The formed precipitate was filtered and washed with ethanol and water. The thiourea derivatives were recrystallized from ethanol and were obtained in enough purity, and no further purifications were needed.

Synthesis of 1-(4-(methylselanyl)phenyl)-3-phenylthiourea (DS036). Compound **DS036** was synthesized from methyl 4-(methylselanyl)aniline (**4**) (1 mmol, 187 mg) and phenyl isothiocyanate (1.2 mmol, 162 mg). The reaction was followed by TLC (EtOAc/hexane 1:2; $R_f=0.25$) and isolated as a white solid with 87% yield (280.1 mg). Compound **DS036** was recrystallized from ethanol as white crystals and its MP was 161–162 °C. IR (FT-IR, cm^{-1}): 3199, 3025, 3001, 1685, 1599, 1522, 1449; ^1H NMR (400 MHz, DMSO) δ 9.80 (d, $J=3.9$ Hz, 2H, 2NH), 7.51 (d, $J=7.8$ Hz, 2H, Ar-H), 7.46–7.33 (m, 6H, Ar-H), 7.15 (t, $J=7.3$ Hz, 1H, Ar-H), 2.36 (s, 3H, SeCH_3). ^{13}C NMR (101 MHz, DMSO) δ 180.03, 139.90, 138.13, 130.37, 128.94, 127.24, 125.02, 124.95, 124.15, 7.38; MS (ESI): m/z = found 345.0 ($\text{M}^+ + \text{Na}$), 321 ($\text{M}^+ - \text{H}$), 323 ($\text{M}^+ + \text{H}$); calcd. 322.0

Synthesis of 1-(4-(benzylselanyl)phenyl)-3-phenylthiourea (DS038). Compound **DS038** was synthesized from 4-(benzylselanyl)aniline (**5**) (1 mmol, 263 mg) and phenyl isothiocyanate (1.2 mmol, 162 mg). The reaction was followed by TLC (EtOAc/hexane 1:2; $R_f=0.25$) and isolated as a white solid with 89% yield (354 mg). Compound **DS038** was recrystallized from ethanol as grey crystals and its MP was 156–158 °C. IR (FT-IR, cm^{-1}): 3198, 3022, 3000, 1599, 1588, 1522, 1449; ^1H NMR (400 MHz, DMSO) δ 9.84 (s, 2H, 2NH), 7.52–7.41 (m, 6H, Ar-H), 7.35 (t, $J=7.8$ Hz, 2H, Ar-H), 7.31–7.25 (m, 4H, Ar-H), 7.21 (td, $J=5.6, 2.4$ Hz, 1H, Ar-H), 7.14 (dd, $J=15.9, 8.5$ Hz, 1H, Ar-H), 4.22 (s, 2H, SeCH_2). ^{13}C NMR (101 MHz, DMSO) δ 179.92, 139.84, 139.25, 139.07, 132.86, 129.28, 128.95, 128.82, 127.24, 125.69, 124.98, 124.51, 124.14, 31.43; MS (ESI): m/z = found 421.0 ($\text{M}^+ + \text{Na}$), 397 ($\text{M}^+ - \text{H}$), 399 ($\text{M}^+ + \text{H}$); calcd. 398.04.

Electrochemical corrosion inhibition measurements (EIS and PDP). The carbon steel samples used in the EIS and PDP experimentations. All experimental runs were performed with the assistance of an electrochemical cell three-electrode system, which was connected to a Gamry potentiostat/galvanostat/ZRA (Reference 600+) electrochemical workstation at a 298 K. The working electrode was made of carbon steel, the counter electrodes were made of platinum sheet, and the reference electrode was made of silver/silver chloride (Ag/AgCl). EIS examination was achieved in a potentiostatic circumstance at a frequency range of 0.1 Hz to 100 kHz with a 10 mV AC signal amplitude and at open circuit potential (E_{OCP}). The optimized EIS response was fitted using the Z-view software version 3.4. Following the EIS optimization, the PDP measurements were done under the same optimized conditions, where the potential was swept at a rate of 1.0 mV s^{-1} at E_{OCP} principally from ± 250.0 mV versus E_{OCP} . The procedure of the LPR corrosion rate tests was similar to those defined in our previous work¹⁰. For each run of the experiment, three duplicate readings were recorded.

DFT calculations and MC simulations. We used the DMOL3 program³⁰ from the Materials Studio package³¹, which is intended for the implementation of large-scale density functional theory (DFT) computations, to perform cluster calculations. Calculations of DFT semi-core pseudopotentials (DSPP) were done using double numerical basis sets and polarization functional theory (DNP). The 6-31G Gaussian basis sets and the DNP basis sets are of equivalent quality^{32,33}. Based on the generalized gradient approximation (GGA), the RPBE functional³⁴ is currently the best exchange–correlation functional³⁵ and is used to account for the effects of electron exchange and correlation. There were no symmetry restrictions when performing the geometric optimization.

By conducting Monte Carlo experiments on the exterior of Fe (110), the adsorption locator revealed the suitable adsorption formations of the protonated forms of the organoselenium base thiourea derivatives for MC simulations³⁶. The particle energy of the thiourea derivatives was improved using the Forcite classical simulation engine³⁷. This was done to calculate the ability of the organoselenium derivatives to inhibit. The organoselenium derivatives, HCl, and external Fe (110) were all adsorbed within a periodic boundary tuning in a simulated box with dimensions of 24.82°A × 24.82°A and 38.24°A. The universal simulation studies with a force field were operated to simulate the adsorption performance of organoselenium base thiourea derivatives on the surface of Fe (110).

Results and discussions

Synthesis of the Se-based thiourea derivatives. 1-(4-(Methylselanyl)phenyl)-3-phenylthiourea (**DS036**) and 1-(4-(benzylselanyl)phenyl)-3-phenylthiourea (**DS038**) were prepared in good yields from the reaction of phenyl isothiocyanate with 4-(methylselanyl)aniline (**4**) and 4-(benzylselanyl)aniline (**5**), respectively (Fig. 2).

Tafel curve measurements. The corrosion current (j_{cor}) considerably decreased after the corrosion inhibitors **DS036** and **DS038** were added, and the corrosion potential (E_{cor}) likewise changed noticeably in either a negative or positive direction, as seen by the Tafel polarization plots in Fig. 3. In comparison to the uninhibited diagram, the form of the remaining anode area curve is extremely important in addition to the polarization curve with a **DS036** and **DS038** concentration of 0.002 mM. The polarization curve's slope quickly increases in the Tafel curve curves at concentrations of 1.0 mM. The shoulder in the polarization curve is associated with the adsorption complexity and desorption route of the active component in the medium and the hindering anode and cathode reaction mechanism³⁸. The cathode region of all the polarization curves has a shape that is remark-

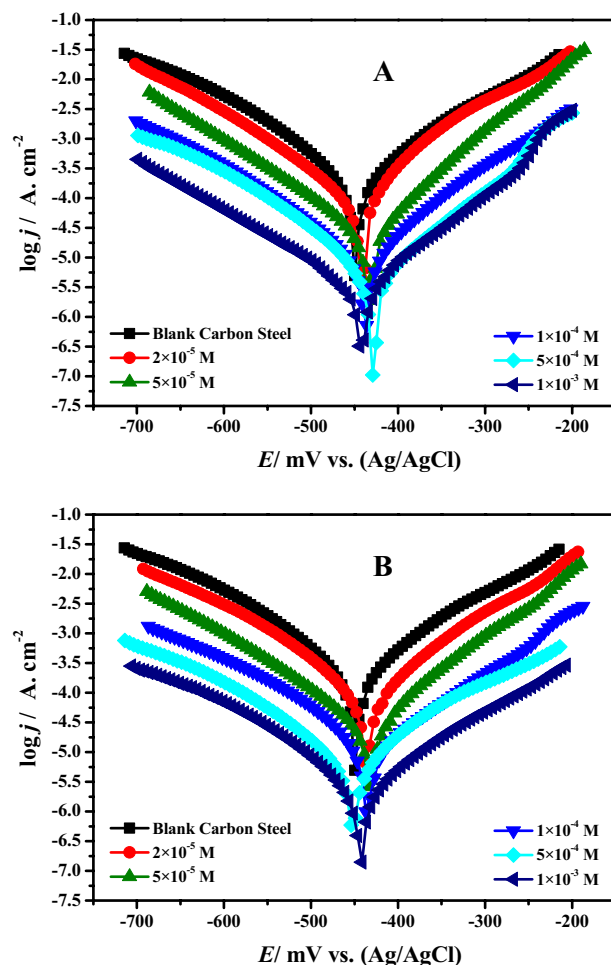


Figure 3. PDP plots for C-steel in molar HCl solution without and with different concentrations of OSe-based thiourea compounds (a) DS036 and (b) DS038.

ably similar, which demonstrates that the addition of the OSe derivatives DS036 and DS038 has no effect on the reaction mechanism of dissolved oxygen reduction. As the DS036 and DS038 dose upsurges, the j_{cor} in the cathode area regularly declines, which designates that this barrier layer adsorbed by DS036 and DS038 on the C-steel surface could decrease the efficient center of the reduction of O_2 on the metal interface, and with the upsurge in DS036 and DS038 dose, the development of a thicker protective layer will cause less active centers of oxygen reduction, resulting in inferior j_{cor} .

The corrosion current of the C-steel electrode gradually decreased when the concentration of DS036 and DS038 is low (0.02 mM), indicating that only a small number of DS036 and DS038 compounds attach to the C-steel surface at this time. Although there is a slight corrosion inhibition effect, this is not acceptable to alter the reaction mechanism of the C-steel anode metal dissolution. This behavior matches the occurrence of a diffusion film on the C-steel surface in the EIS studies, which will be discussed later. When the DS036 and DS038 dose exceeds 0.50 mM, there are enough DS036 and DS038 molecules in the medium to form a denser protective coating on the surface of the C-steel, preventing the C-steel from deterioration.

The cathode and anode currents of all polarization curves containing DS036 and DS038 tend to drop, which shows that these molecules block their response to the cathode and anode regions of the C-steel surface. As a result, these molecules are mixed corrosion inhibitors for C-steel.

In order to reduce error when using the Tafel extrapolation method to fit the polarization curve data, the anode region of the polarization curve does not take part in the fitting. This is because the iron on the surface of the C-steel in the anode region will dissolve to a certain extent and the metal surface is relatively rough³⁹. The j_{cor} values are fitted using the cathode region's polarization curve. The appropriate parameters are revealed in Table 1 which contains E_{cor} , j_{cor} , β_c , and β_a (cathodic and anodic Tafel slope), and the inhibition efficiency ($\eta_i/\%$) from the Tafel polarization plot is intended by the following Eq.⁴⁰:

$$\eta_i/\% = \left(\frac{j_{cor,0} - j_{cor,i}}{j_{cor,0}} \right) \times 100 \quad (1)$$

Inhibitor code	C_i (mol L ⁻¹)	j_{cor} ($\mu\text{A cm}^{-2}$) \pm SD	E_{cor} (mV) (SCE)	β_a (mV dec ⁻¹)	$-\beta_c$ (mV dec ⁻¹)	θ	μ_p %
Blank	0.0	821.7 \pm 31.2	- 450.5	91.75	163.92	-	-
DS036	2.0×10^{-5}	473.87 \pm 24.3	- 440.6	84.13	173.66	0.4233	42.33
	5.0×10^{-5}	321.61 \pm 19.4	- 435.4	86.01	169.69	0.6086	60.86
	1.0×10^{-4}	178.55 \pm 11.5	- 434.8	81.07	174.87	0.7827	78.27
	5.0×10^{-4}	68.28 \pm 5.2	- 429.2	78.68	172.16	0.9169	91.69
	1.0×10^{-3}	27.52 \pm 2.1	- 442.8	85.93	175.71	0.9665	96.65
DS038	2.0×10^{-5}	431.14 \pm 22.6	- 438.4	82.27	176.87	0.4753	47.53
	5.0×10^{-5}	297.04 \pm 17.7	- 433.5	85.85	179.94	0.6385	63.85
	1.0×10^{-4}	146.34 \pm 9.8	- 437.6	90.01	180.62	0.8219	82.19
	5.0×10^{-4}	41.33 \pm 3.1	- 452.8	88.96	178.28	0.9497	94.97
	1.0×10^{-3}	11.99 \pm 1.5	- 439.4	88.48	176.18	0.9854	98.54

Table 1. PDP plots for C-steel in molar HCl solution without and with different concentrations of OSe-based thiourea compounds (DS036 and DS038) at 298 K.

Amongst them, j_{cor0} , and j_{cori} are the corrosion current densities for C-steel electrodes in the blank without and with DS036 and DS038 molecules, respectively. As can be observed from Table 1, with the upsurge of DS036 and DS038 doses, the j_{cor} of C-steel is also decreased, and the η_i % is progressively enhanced. When the dose of DS036 and DS038 reached 0.002 mM, the η_i % of DS036 and DS038 was meaningfully improved, and the η_i % reached 42.33 and 47.53%, respectively. When the DS036 and DS038 dose reaches 1.0 mM, the j_{cor} are 27.52, and 11.99 $\mu\text{A}/\text{cm}^2$, and the η_i % reaches 96.65, and 98.54%, respectively. The outcomes are significantly consistent with those of EIS.

Impedance analysis. EIS was carried out to further examine the mechanism of DS036 and DS038 molecules' corrosion inhibition on C-steel. The OCP had reached a stable condition following 60 min of immersion of the C-steel specimen in molar HCl without and with various concentrations of DS036 and DS038 at 298 K. Based on this, the Nyquist and Bode plots for the C-steel electrode at a constant OCP were obtained and are shown in Figs. 4, 5. Figures 4, and 5 display the obtained EIS findings in Nyquist and Bode modules, respectively. This Figure clearly shows that all impedance spectra have a single capacitive loop, which demonstrates that the charge transfer process is primarily responsible for controlling the corrosion of C-steel in molar HCl with and without inhibitors and is regularly associated with the double-layer performance⁴¹. Additionally, these diagrams are identical for all concentrations tested, showing that the corrosion mechanism is unchanged⁴². The frequency dispersion of interfacial impedance may also be to blame for the fact that these Nyquist graphs are not perfect semicircles⁴³. Chemical inhomogeneity, surface coarseness, and the adsorption-desorption process of inhibitive molecules on C- steel surfaces all contribute to this phenomenon⁴⁴. Additionally, the semicircle's diameter in the occurrence of the inhibitors DS036 and DS038 is larger than that observed in a molar HCl (blank solution) and grows with a growing inhibitor dose, which might be related to the expansion of the surface coverage of inhibitive compounds on the C-steel interface.

Figure 5 shows the appropriate Bode impedance modules for C-steel electrodes immersed in molar HCl with and without various inhibitor doses at its OCP. The increase of absolute impedance at low frequencies in the Bode plot confirms the higher protection with the increasing inhibitor concentration⁴³. The concentration of DS036 and DS038 inhibitors in 1.0 M HCl is increased, as indicated by an increase in absolute impedance. This indicates superior inhibitive behavior because more inhibitor molecules are adsorbed on the C-steel surface at greater concentrations⁴⁵.

Figure 6 shows the comparison of Nyquist (A, B) and Bode diagrams (C, D) (black points) measured for steel specimens immersed in HCl and the simulated (red lines) for inhibited and uninhibited systems. An electrochemical equivalent circuit (EEC) was used in the fitting for the data for uninhibited electrodes (E) and inhibited electrodes (F), where R_s is the electrolyte resistance, CPE (Y_0 , α) denotes a constant-phase element, and R_p denotes the polarization resistance ($R_p = R_{ct}$ (charge transfer resistance) + R_f (film resistance)) in addition to the film capacitance (C_{ads}), and inhibitor resistance (R_{ads}) in the case of the inhibited system.

The element of CPE is utilized to clarify the capacitance semi-circle depression, which matches surface inhomogeneity resulting from impurities, surface coarseness, grain boundaries, displacements, additive adsorption, development of porous film, etc. The impedance CPE function is characterized by the following Eqn.⁴⁶:

$$Z_{CPE} = \frac{1}{Q(j\omega)^\alpha} \quad (2)$$

where j represents the imaginary number ($j^2 = -1$), Q signifies the CPE magnitude, and ω characterizes the angular frequency. α epitomizes the deviation restriction ($-1 \leq \alpha \leq +1$), which has the significance of a phase shift. The CPE denotes a pure resistor when $\alpha = 0$, a pure capacitor when $\alpha = +1$, and an inductor when $\alpha = -1$ ⁴⁷. Additionally, the following equation was used to get the double-layer capacitances, C_{dl} , for a circuit that has a CPE⁴⁸:

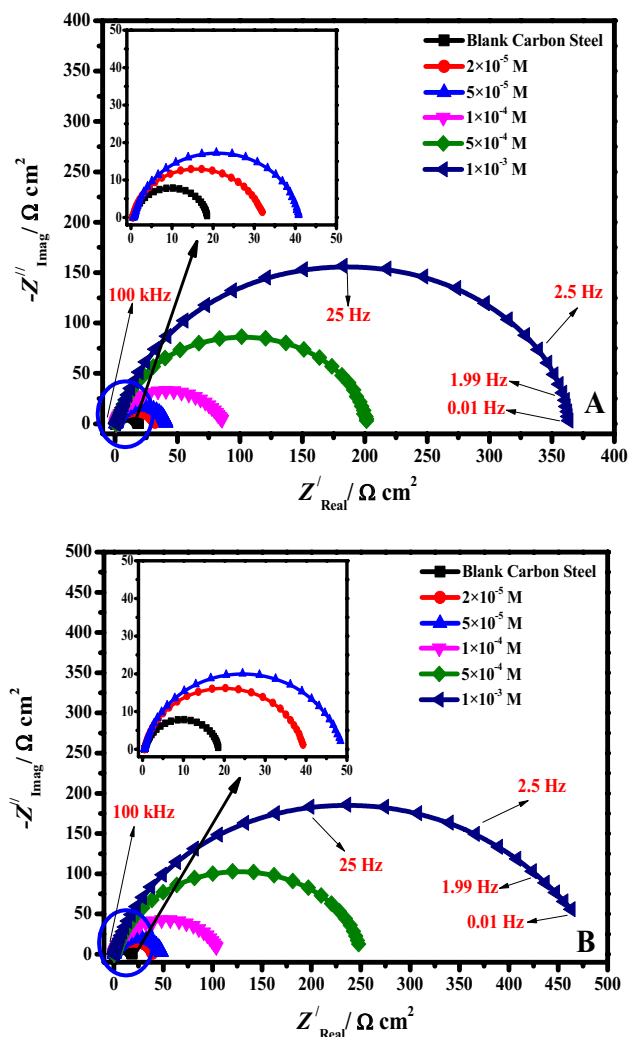


Figure 4. Nyquist plot of C-steel electrode in the blank molar HCl solution and with the addition of varying concentrations (A) DS036 and (B) DS038 at 298 K.

$$C_{dl} = Q(2\pi\omega_{\max})^{\alpha-1} \quad (3)$$

where ω_{\max} is the maximum frequency value at the imaginary part of the EIS range. The electrochemical parameter values such as n , R_s , R_p , C_{dl} , Y_0 , and $\eta_E/\%$ (inhibition capacity) of DS036 and DS038 were attained from EIS and recorded in Table 2. In the occurrence of DS036 and DS038, the values of n are found to be in the range of 0.792 to 0.884 and these values are more than the uninhibited solution (0.717). The higher n values in the inhibitor-containing systems exhibit that the DS036 and DS038 molecules produce a protective film over the C-steel surface and progress their homogeneity¹⁰. As the concentration of the inhibitor rises, the R_p values upsurge and the C_{dl} values decrease. The uppermost R_p (363.64 $\Omega \text{ cm}^2$ for DS036 and 463.15 $\Omega \text{ cm}^2$ for DS038) has been found at an optimal dose (1.0 mM). The adsorption of inhibitors results in a rise in R_p values, suggesting a reduction in the exposed surface. However, a drop in C_{dl} , which might be brought on by a reduction in the local dielectric constant and/or a rise in the thickness of the electrical double layer, suggests that the DS036 and DS038 inhibitors act by adsorption at the metal/medium interface. When the concentration of these OSe-based derivatives exceeds 1.0 mM, the values of inhibitory efficiency rise to 94.9% for DS036 and 95.9% for DS038. These findings demonstrate once more that the prepared compounds have effective C-steel inhibitory performance in HCl solution and $\eta_E/\%$ follows the order: DS038 > DS036. It is important to note that the inhibitory efficiencies determined by electrochemical measurements are essentially in agreement with those determined by PDP, as indicated in Table 1.

Effect of temperature. The effect of temperature on C-steel corrosion in an HCl medium in the absence and existence of different inhibitor doses has been examined at the temperature range (298–328 K) using the EIS method. Figure 7 shows the relationship between inhibition efficiency and temperature in (A) DS036 and (B) DS038 at different concentrations. The inhibition efficiency for DS036 was changed from 42.3, and 96.6% at

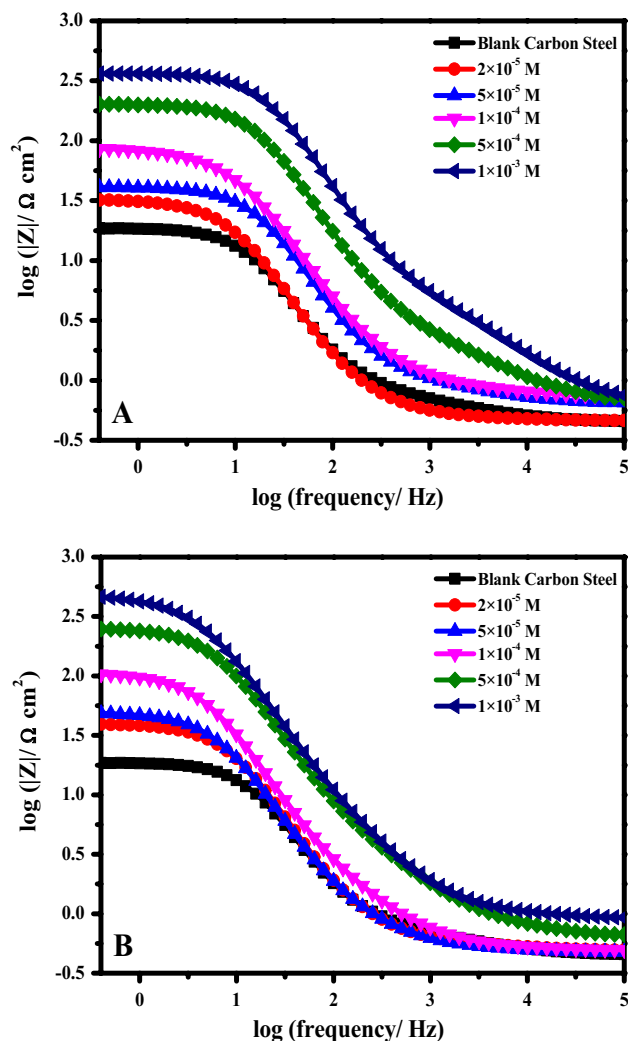


Figure 5. Bode plot of C-steel electrode in the blank molar HCl solution and with the addition of varying concentrations (A) DS036 and (B) DS038 at 298 K.

298 K to 39.1, and 98.2% at 328 K, in the presence of 2.0×10^{-5} and 1.0×10^{-3} M, respectively (Fig. 7A). While, in the presence of the DS038 compound, the inhibition efficiency was altered from 47.5, and 98.54% at 298 K to 42.2, and 99.1% at 328 K in the presence of 2.0×10^{-5} and 1.0×10^{-3} M, respectively, respectively (Fig. 7B). Consequently, DS036 and DS038 inhibitor systems still display remaining protection performance to protect C-steel from corrosion by producing an adsorption layer on the metal interface even at higher temperature²¹. By comparing the activation energy (E_a) in the presence and absence of the corrosion inhibitor, some important details concerning the adsorption mechanism of the inhibitor can be learned. The E_a values in the presence of organoselenium thiourea derivatives are seen to increase as the inhibitor concentration increases. The data demonstrate that the investigated electrode's E_a values in the analyzed corrosive media in the presence of DS036 and DS038 (35.25 and 40.65 for DS036 and DS038 respectively) are greater than those in the uninhibited medium (12.97 kJ/mol). As a result, the presence of an inhibitor raises the activation energy barrier of the tested electrodes' corrosion and hence lowers the corrosion rate. We can draw the conclusion that the increase in corrosion activation energy in the presence of DS036 and DS038 is commonly attributed to the development of a physical-character protective adsorption layer. The inhibitor system is physically adsorbed at lower temperatures, whereas chemisorption is more advantageous as the temperature rises²¹.

Effect of immersion time. In order to examine the stability of the adsorptive inhibitor film with time, the influence of exposure time on the corrosion rate was studied. The change of the corrosion rate with duration time for C-steel in 1.0 M blank HCl and containing 1.0×10^{-3} M of DS036 and DS038 at 25 °C was presented in Fig. 8. After one hour of immersion in the corrosive solution, the organoselenium thiourea compounds were introduced because at this point the E_{cor} became stable. CR was discovered to range between 2.62 and 4.76 mm/year in the blank medium. The CR of C-steel steadily increases with immersion duration in the blank media, as is shown in Fig. 8. The CR of C-steel was clearly expressively reduced by the addition of the synthetic organoselenium

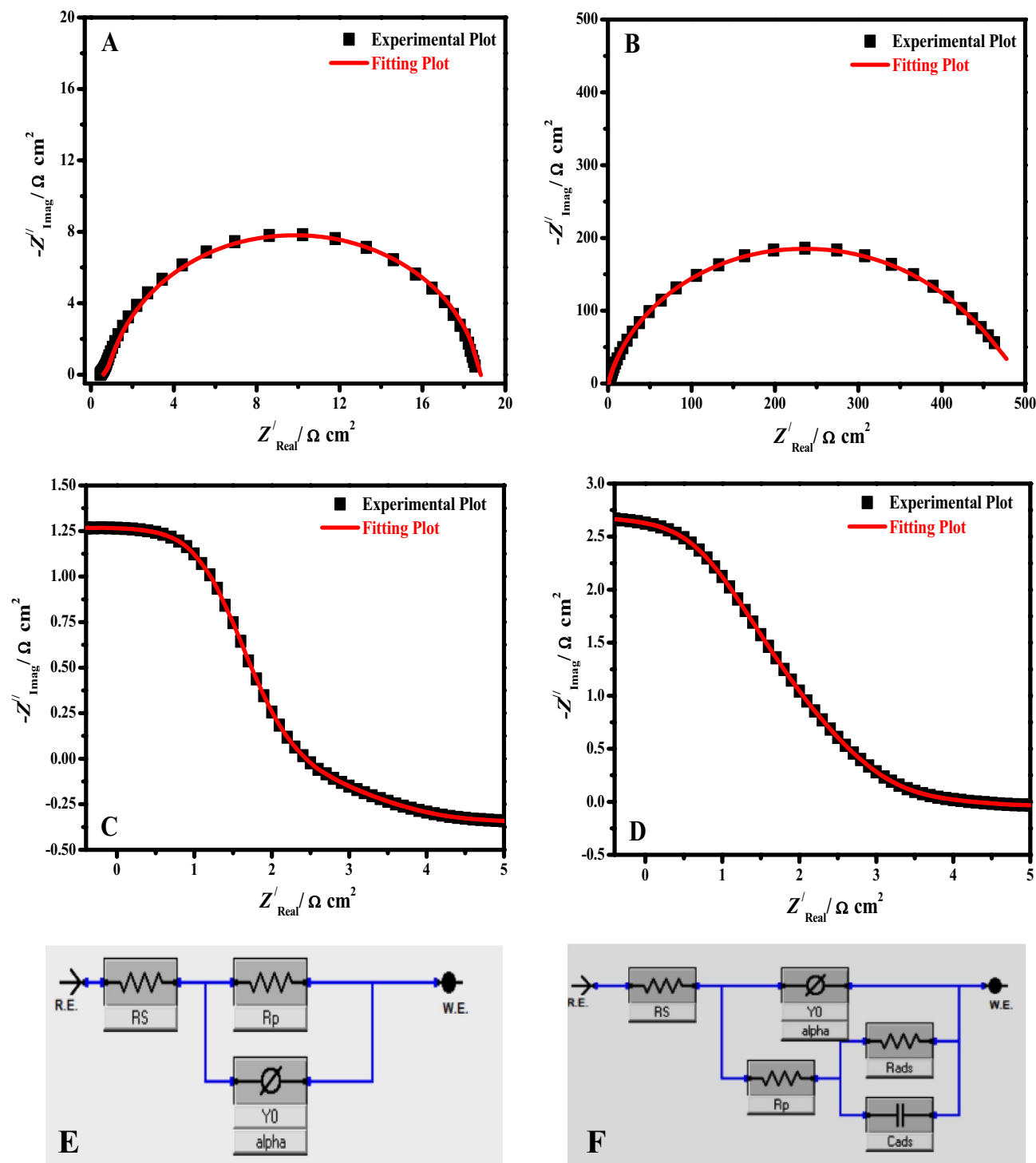


Figure 6. Comparison of Nyquist (A, B) and Bode diagrams (C, D) (black points) measured for steel specimens immersed in HCl and the simulated (red lines) for inhibited and uninhibited systems. EEC used in the fitting of data for the uninhibited electrode (E) and inhibited electrode (F).

nium thiourea compounds. The CR reduced from 4.62 to 0.21 and 0.06 mm/year in the presence of 1.0×10^{-3} M of DS036 and DS038, respectively, after 20 h of immersion. It might be accredited to its adsorption and formation of a protective layer on the metallic surface. During 2 to 20 h of exposure, the CR in DS036 and DS038-inhibited HCl is practically constant, showing that the adsorption film for DS036 and DS038 is stable and does not rupture with time.

Adsorption isotherm studies. Assuming that the inhibitory effect is primarily caused by adsorption at the metal/solution contact will allow us to determine the adsorption isotherm. The adsorption isotherm can

Inhibitor codes	C_{inh} (mol/L)	R_s (Ω cm ²)	R_p (Ω cm ²) \pm SD	C_{dl} (F cm ⁻²) $\times 10^{-6}$	Q_{CPE}		χ^2 $\times 10^{-4}$	θ	η_E (%)
					Y_0 ($\mu\Omega^{-1}$ s ⁿ cm ⁻²)	n			
Blank	0.0	0.45	18.53 \pm 1.1	710.9	90.39	0.717	5.21	–	–
DS036	2.0×10^{-5}	0.46	31.72 \pm 3.5	285.7	56.84	0.792	4.28	0.415	41.5
	5.0×10^{-5}	0.65	40.79 \pm 4.2	230.9	40.34	0.814	4.29	0.545	54.5
	1.0×10^{-4}	0.77	84.73 \pm 6.5	129.7	29.64	0.856	5.16	0.781	78.1
	5.0×10^{-4}	0.79	201.41 \pm 12.4	55.5	11.86	0.835	5.25	0.908	90.8
	1.0×10^{-3}	0.85	363.64 \pm 18.8	49.7	4.52	0.856	5.18	0.949	94.9
DS038	2.0×10^{-5}	0.49	39.29 \pm 2.9	226.9	43.37	0.801	5.11	0.528	52.8
	5.0×10^{-5}	0.57	48.42 \pm 4.6	187.4	31.12	0.818	3.79	0.617	61.7
	1.0×10^{-4}	0.69	103.73 \pm 8.7	117.1	22.86	0.844	4.97	0.821	82.1
	5.0×10^{-4}	0.76	247.91 \pm 16.8	29.7	9.14	0.860	4.83	0.925	92.5
	1.0×10^{-3}	0.98	463.15 \pm 24.2	20.5	3.44	0.884	5.14	0.959	95.9

Table 2. EIS corrosion parameters of C-steel electrode in the blank molar HCl solution and with the addition of varying concentrations **DS036** and **DS038** at 298 K.

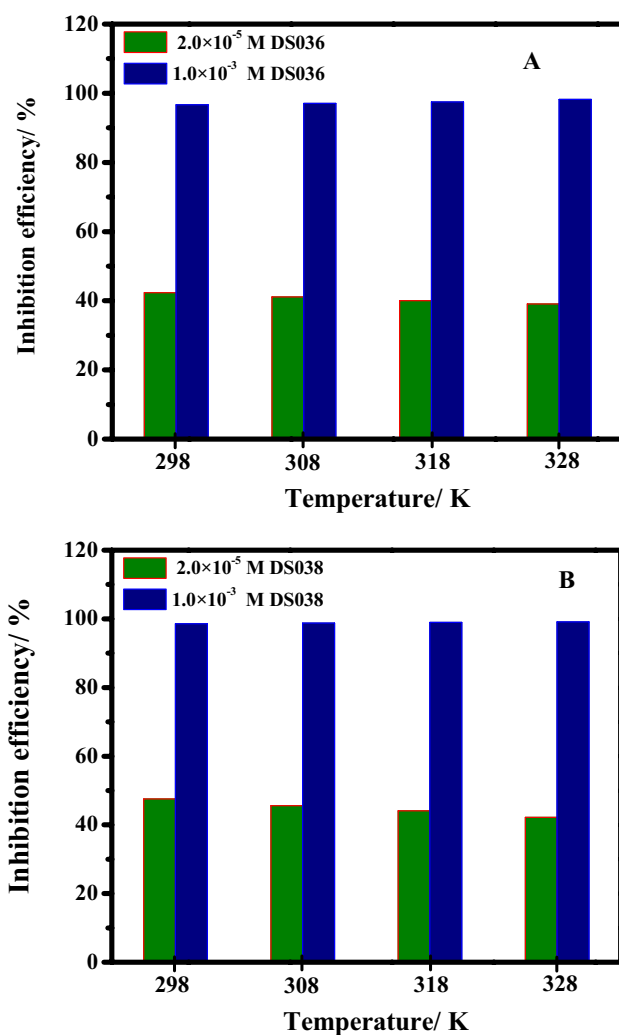


Figure 7. Relationship between inhibition efficiency and temperature in (A) DS036 and (B) DS038 at different concentrations.

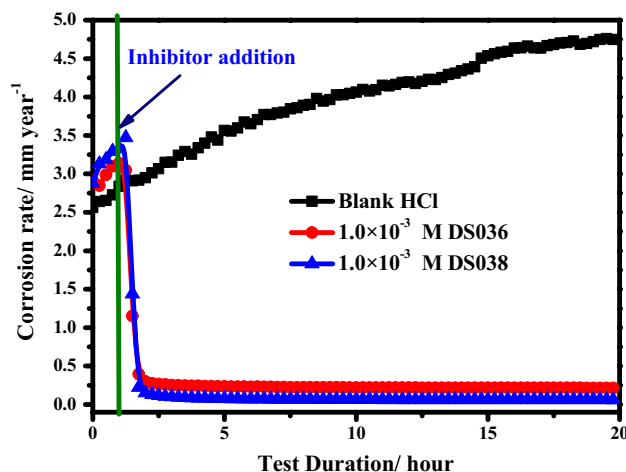


Figure 8. Variant of the corrosion rate with duration time for C-steel in 1.0 M blank HCl and containing 1.0×10^{-3} M of DS036 and DS038 at 25 °C.

give fundamental details on the adsorption of inhibitors on the metal surface. The fractional surface coverage values (θ) as a function of inhibitor concentration must be ascertained in order to derive the isotherm. The surface coverage (θ) values could be simply measured from the PDP studies by the ratio inhibition efficiency/100. Therefore, empirical research is required to establish which isotherm best describes the adsorption of inhibitors on the surface of C-steel. Numerous adsorption models such as Langmuir, Frumkin, Freundlich, and Temkin isotherms were characterized. Among the different models of adsorption isotherms tried, the most appropriate one was selected with the help of the correlation coefficient (R^2) (Table S1). Langmuir isotherm was found to be the most fitting to the experimental findings, with all correlation coefficient values very close to unity, confirming that the adsorption process of OSe-based compounds on C-Steel in 1.0 M HCl follows Langmuir isotherm model. The isotherm model of Langmuir is described by the following Eqn.⁴⁹:

$$\left(\frac{C_{inh}}{\theta}\right) = \left(\frac{1}{K_{ads}}\right) + C_{inh} \quad (4)$$

where K_{ads} and C_{inh} are the adsorption equilibrium constant and the inhibitor molar concentration. Figure 9 shows a straight line in the plot of the $\log(C_{inh}/\theta)$ vs. C_{inh} . The linear regression coefficients (R^2) are nearly equivalent to 0.999 for DS036, and DS038 inhibitors, which indicates that the examined compounds adhere to Langmuir's adsorption isotherm during adsorption in 1.0 M HCl solution. The adsorption-free energy (ΔG_{ads}^0) is interrelated to the K_{ads} with the following Eqn.^{50,51}:

$$\Delta G_{ads}^0 = -RT \ln(55.5K_{ads}) \quad (5)$$

where the value 55.5 is the molar concentration of H_2O . The values of K_{ads} and ΔG_{ads}^0 were calculated at 298 K and. The K_{ads} values were found to be 9.91×10^3 and $10.02 \times 10^3 M^{-1}$ for DS036, and DS038 inhibitors, respectively. Moreover, the ΔG_{ads}^0 values were found to be -32.74 and $-32.81 kJ mol^{-1}$ for DS036, and DS038 inhibitors, The instability of the adsorbed layer on the C-steel surface and the spontaneity of the adsorption process were both established by the negative values of ΔG_{ads}^0 . Additionally, the DS038 inhibitor's high ΔG_{ads}^0 value demonstrated that it is more strongly adsorbed on the C-steel surface in 1.0 M HCl than the DS036 molecule. This is well-aligned with the range of inhibitory efficiency values discovered using electrochemical methods. It is common knowledge that values of ΔG_{ads}^0 the order of $-20 kJ mol^{-1}$ or below suggest physisorption, while values more negative than $-40 kJ mol^{-1}$ include the sharing or electron transfer from the inhibitor molecules to the steel surface to form a coordinate type of bond (chemisorption). In this report, the ΔG_{ads}^0 values ranging between -20 and $-40 kJ mol^{-1}$ obviously specify its combined chemical and physical adsorption on the C-steel interface⁵².

Surface morphology by FE-SEM. FE-SEM analysis of C-steel conducted after 20 h of exposure to blank HCl (A) and 1.0 103 M DS038 is shown in Fig. 10A, B. The metal surface was severely corroded and degraded, with some pits and deep cavities, as evidenced by close examinations of the FE-SEM image acquired in the absence of the DS038 inhibitor (Fig. 10A). The metal sample has a superior morphology and smooth interface compared to the C-steel surface immersed in the blank medium when DS038 inhibitor is present (Fig. 10B). According to this, using DS038 inhibitor slows down the corrosion rate by preventing C-steel dissolving. This indicates effective corrosion inhibition.

DFT studies. Figure 11 shows the optimized structures, including the HOMO and LUMO distributions for organoselenium base thiourea derivatives. Table 3 presents the corresponding quantum chemical descriptors. According to frontier orbital theory, the HOMO and LUMO energies^{53,54} explain the donor or acceptor interac-

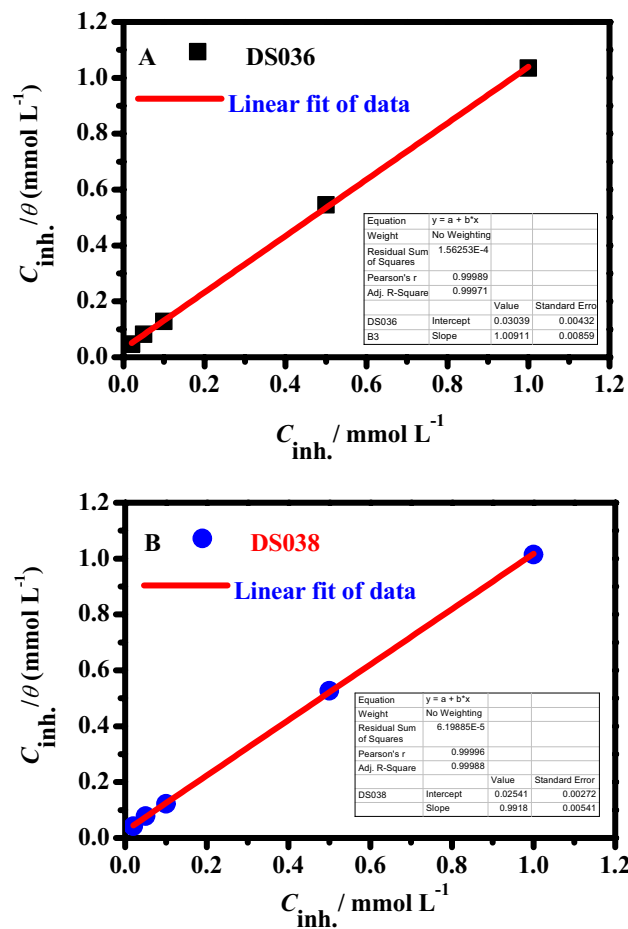


Figure 9. Adsorption model of Langmuir isotherm of inhibitors (DS036, and DS038) on the C-steel surface in molar HCl at 298 K.

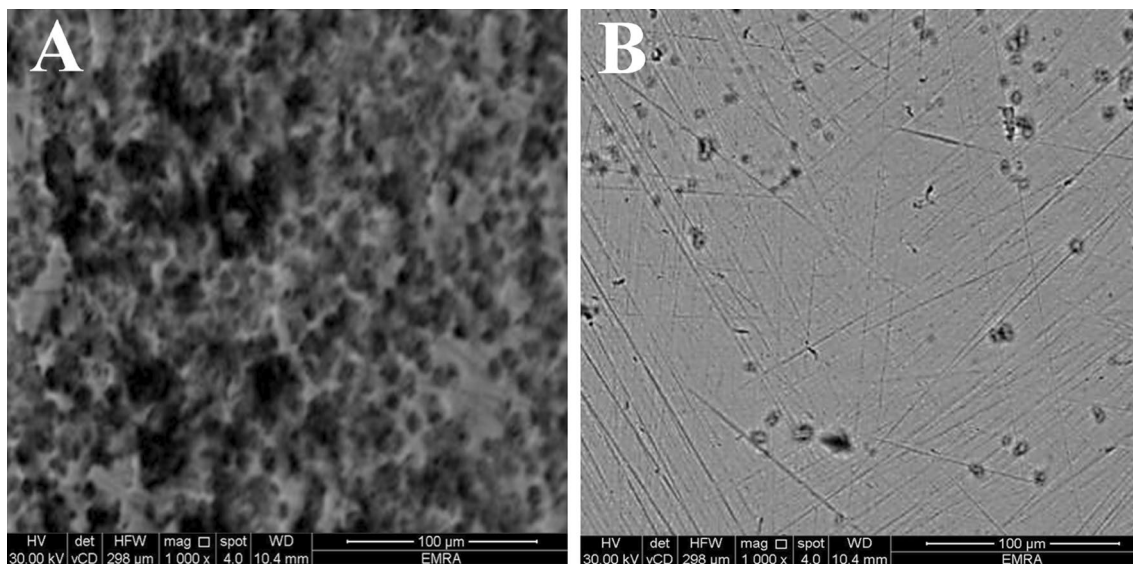


Figure 10. FE-SEM pictures for C-steel in blank 1.0 M HCl (A) and containing 1.0×10^{-3} M DS038 compound after 20 h of immersion.

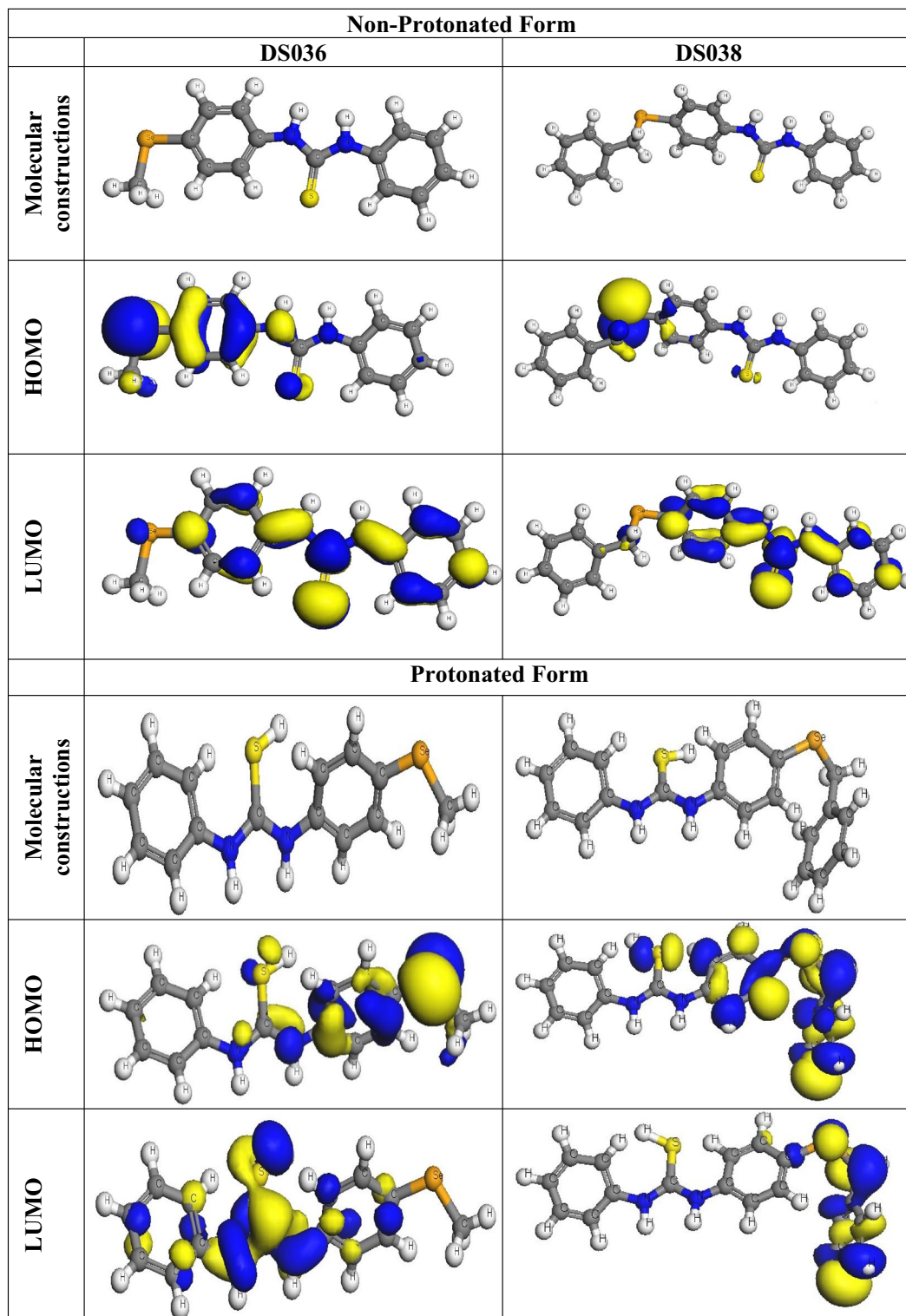


Figure 11. The optimized molecular constructions, HOMO, and LUMO for DS036 and DS038.

tions at the interface between the inhibitor molecule and metal exterior. Consequently, high and low readings for E_{HOMO} and E_{LUMO} , respectively, point to a corrosion prohibition that is strengthened by the presence of the compounds under investigation. In Table 3, DS038 has a higher HOMO value of -4.56 eV when compared with DS036 (-5.33 eV) while in protonated form were 5.06 and 5.19 eV for DS038 and DS036 respectively. As shown in Fig. 11, the HOMO levels for DS036 were located at the seloxy, thiole, imine, and one of the phenyl rings, suggesting that the nitrogen, Se, and sulfur atoms were the favored positions for electrophilic attacks on the metal exterior. The HOMO levels in DS038 were found at the seloxy, thiole, and imine positions, implying

Compound		E_{HOMO} (eV)	E_{LUMO} (eV)	ΔE (eV)	IE	EA	η	σ	χ	ΔN	μ
Non-Protonated Form	DS036	-5.33	-1.66	3.67	5.33	1.66	1.84	0.54	3.50	0.36	3.51
	DS038	-4.56	-1.61	2.75	4.56	1.61	1.48	0.68	3.09	0.60	4.15
Protonated Form	DS036	-5.19	-4.35	0.84	5.19	4.35	2.38	0.42	4.77	0.06	3.71
	DS038	-5.06	-4.37	0.69	5.06	4.37	2.89	0.35	4.72	0.14	4.48

Table 3. DFT parameters of **DS036** and **DS038** compounds.

that the nitrogen, Se, and sulfur atoms were the preferred positions for electrophilic attacks on the metal exterior. This could increase the potency of the prohibition caused by the **DS036** and **DS038** derivatives' adsorption on the steel surface. In contrast, the E_{LUMO} value was -1.61 eV for **DS038** (Table 3), which was less than -1.66 eV for **DS036**. We observe that small differences in values between the inhibitors demonstrate the inhibitors' low inhibition activity differences, where better inhibition efficiency was observed for **DS038**. These results show that protonated species have a stronger propensity than non-protonated molecules to adsorb on the surface of the C-steel.

Important parameters, including the energy gap (ΔE), HOMO, LUMO, global hardness (η), softness (σ), electronegativity (χ), and electron transfer fraction (ΔN) were determined from the DFT calculation from the Eqns. 6–11^{38,55}.

$$IE = -E_{HOMO} \quad (6)$$

$$EA = -E_{LUMO} \quad (7)$$

$$\eta = \frac{1}{2}(IE - EA) = \frac{1}{2}(E_{LUMO} - E_{HOMO}) \quad (8)$$

$$\chi = \frac{1}{2}(IE + EA) = \frac{1}{2}(-E_{LUMO} - E_{HOMO}) \quad (9)$$

$$\sigma = \frac{1}{\eta} \quad (10)$$

$$\Delta N = \frac{\chi_{Fe} - \chi_{inh.}}{2(\eta_{inh.} + \eta_{Fe})} \quad (11)$$

where the electronegativity was 4.82 eV for Fe has been applied for the calculation of electron transfer (ΔN).

The energy gap (ΔE) is a crucial component in enhancing the organoselenium derivatives' ability to suppress corrosion. Better inhibitory potencies were suggested by lower ΔE values⁵⁶. Table 3 shows that **DS038** has a lower ΔE value than **DS036** (2.75 eV) and 3.67 eV. This suggested a greater propensity for **DS038** adsorption on the outside of the C-steel. The lower values of electronegativity (χ) for **DS038** revealed that **DS038** had a greater capacity to supply electrons to the metal than **DS036**⁵⁷. A compound's stability and reactivity can be used to determine how hard or soft it is. During the adsorption process, soft chemicals, which are more reactive than hard ones, easily supply electrons to a C-steel sample. They function effectively as corrosion inhibitors as a result⁵⁸. The **DS038** has a greater value (0.68), while the **DS036** has a higher value, as indicated in Table 3. (1.84). This demonstrated **DS038** simplicity in supplying electrons to the tested substance. As a result, high potency emerged.

The ΔN values demonstrated a particle's propensity to give electrons to the surface. A high ΔN value indicates that an inhibitor has a greater capacity for electron donation. When ΔN 3.6 is present, the strong electron-contributing ability improves the prohibition performance⁵⁹. The determined values of ΔN are shown in Table 3. The fact that **DS038's** ΔN value was larger (0.60) than **DS036's** (0.36) suggested that **DS038** was more likely to contribute electrons to the sample under study.

A powerful aspect that supports corrosion restriction is the dipole moment⁶⁰. An improvement in the deformation energy and an improvement in the adsorption of an inhibitor on the steel surface are both indicated by an increase in the dipole moment. Therefore, an increase in the dipole moment will boost the effectiveness of the prohibition⁶¹. Table 3 demonstrates that **DS038** has a greater dipole moment (4.15 Debye) than **DS036** (3.51 Debye) while 4.48, 3.71 Debye for **DS038** and **DS036** in the case of protonated form. This demonstrated the increased propensity of **DS038** to adsorb on the C-steel surface, resulting in increased prohibition potency. Indicating that dipole–dipole interactions predominate more in the interaction between the protonated form and the C-steel interface than in the interaction between the C-steel surface and the non-protonated form, the values are higher for the protonated molecules than for the non-protonated molecules. It can be determined that the protonated organoselenium base thiourea derivatives forms are more effective at resisting corrosion than the non-protonated organoselenium base thiourea derivatives forms based on the above-calculated quantum characteristics.

MC simulations. The interactions of the organoselenium base thiourea derivatives with the C-steel surface and the mechanism of adsorption were visualized using MC simulations. The most plausible organoselenium derivative adsorption arrangements on the steel sample are depicted in Fig. 12. The adsorption locator module, which displays the smooth disposition and recommends an improvement in the adsorption with the largest surface coverage, was responsible for achieving this. In addition, Table 4 compiles the results of the Monte Carlo simulations. Table 4 provides the stiff adsorption energies for relaxed adsorbate compounds, relaxed adsorbate compound deformation energies, and relaxed adsorbate compound adsorption energies^{62–67}.

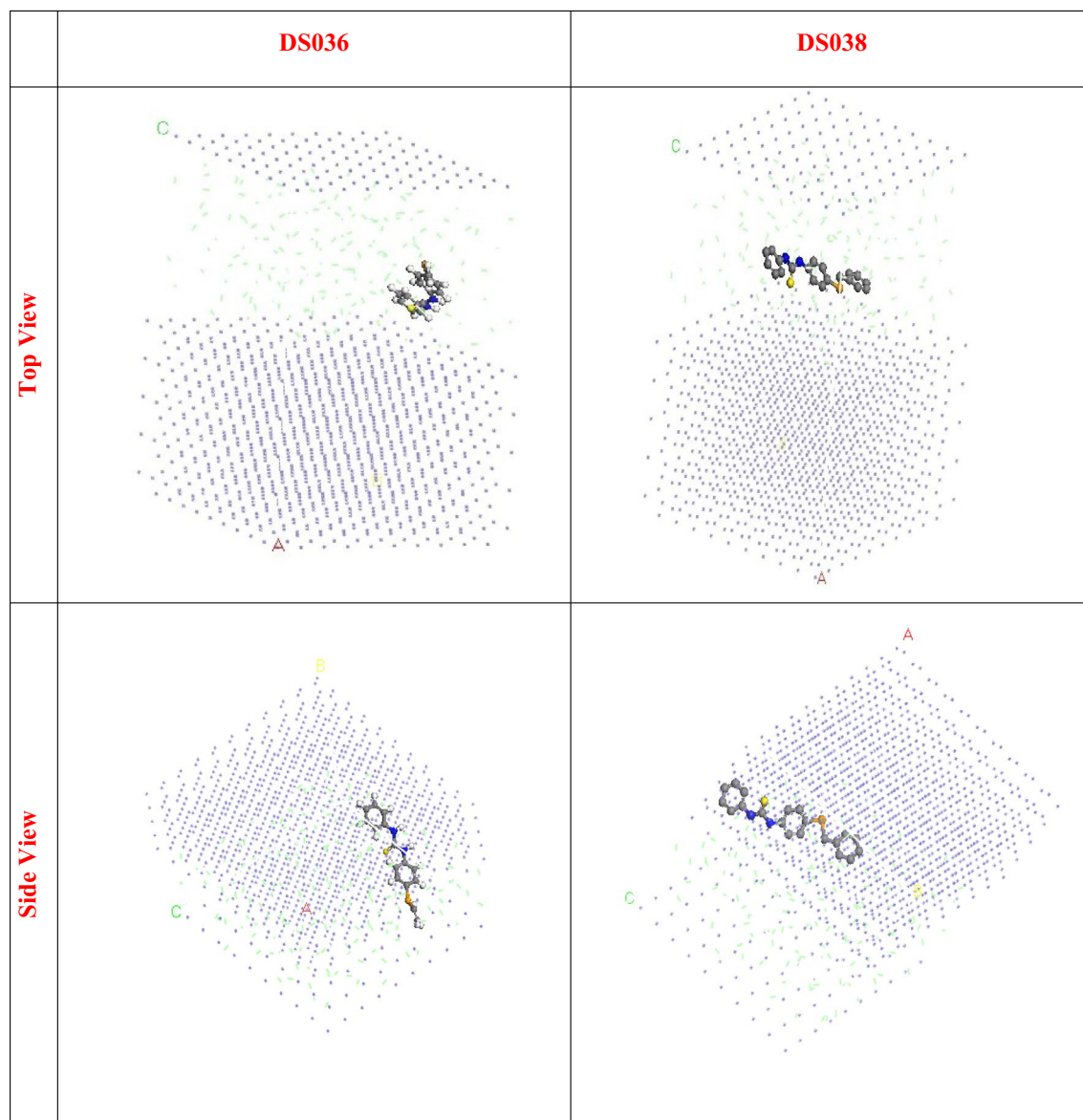


Figure 12. The adsorption locator module achieved the maximal suitable conformation for the adsorption of DS036 and DS038 on Fe (110) substrate.

Compound		Total energy	Adsorption energy	Rigid adsorption energy	Deformation energy	Inhibitor: dE_{ads}/dN_i	HCl: dE_{ads}/dN_i
Non-Protonated Form	DS036	– 362.61	– 407.22	– 407.70	– 487.70	– 44.78	– 2.53
	DS038	– 359.08	– 513.41	– 416.29	– 497.12	– 55.42	– 3.06
Protonated Form	DS036	– 258.59	– 408.54	– 308.92	0.3755	– 36.76	– 2.02
	DS038	– 227.31	– 583.34	– 283.63	0.2872	– 28.27	– 2.49

Table 4. Data and descriptors obtained using the Monte Carlo simulation for the adsorption of DS036, and DS038 compounds on Fe (110).

Compared to **DS036** the **DS038** displayed a greater negative value for adsorption energy ($-513.41 \text{ kcal mol}^{-1}$) ($-407.22 \text{ kcal mol}^{-1}$). This demonstrated that **DS038** adhered to the C-steel surface more strongly than **DS036** did, forming a stable adsorbed barrier that inhibits C-steel corrosion and indicating a stronger prohibition tendency for **DS038** than for **DS036**.

When the energy of the adsorbate was ignored, the dE_{ads}/dN_i figures helped to understand the energy of the metal adsorbate configuration. The higher dE_{ads}/dN_i values for **DS038** ($55.42 \text{ kcal mol}^{-1}$), as opposed to **DS036** ($44.78 \text{ kcal mol}^{-1}$), show that **DS038** had larger adsorption than **DS036**. A further indication that **DS038** and **DS036** have a higher affinity for adsorption than HCl is the fact that HCl molecules have a dE_{ads}/dN_i ratio of $-3.06 \text{ kcal mol}^{-1}$. Thus, **DS038** and **DS036** formed a reliable barrier of protection and were irrevocably adsorbed on the Fe surface. The dE_{ads}/dN_i figures help to clarify the energy of the metal adsorbate arrangement when the energy of the adsorbate was ignored. **DS038** had greater adsorption than **DS036**, as evidenced by the higher dE_{ads}/dN_i values for **DS038** ($-55.42 \text{ kcal mol}^{-1}$) compared to **DS036** ($-44.78 \text{ kcal mol}^{-1}$). In addition, the fact that HCl molecules have a dE_{ads}/dN_i value of $-3.06 \text{ kcal mol}^{-1}$ indicates that **DS038** and **DS036** have a larger affinity for adsorption than HCl. Thus, **DS038** and **DS036** created a solid protective barrier and were definitively adsorbed on the Fe surface. It's interesting to note that these results match the above DFT and empirical results.

Conclusions

OSe-based derivatives were synthesized and their mitigation performance for C- steel in an acidic pickling solution was inspected from both theoretical and experimental characteristics. The obtained results show that these compounds can make a suitable preventing surface and control the corrosion rate. The inhibition efficiencies are 96.65% and 98.54% in the presence of 1.0 mM of **DS036** and **DS038**, respectively. The synthesized OSe-based compounds were mixed-type inhibitors, according to the PD data, and the inhibition efficiency increased with increasing inhibitor doses. The highest R_p ($363.64 \Omega \text{ cm}^2$ for **DS036** and $463.15 \Omega \text{ cm}^2$ for **DS038**) have been found at an optimal dose (1.0 mM). These molecules combined chemisorption and physisorption adsorption onto the surface of the C-steel and followed the Langmuir adsorption isotherms. The effects of immersion time and temperature reinforced further the performance of both synthesized OSe-based compounds. The FE-SEM analysis revealed a smoother electrode surface after the addition of the OSe-based molecules, proving that a shielding film had been formed to shield the steel substrate from contact with aggressive ions. The outcomes of the MC simulations and DFT calculations were in good agreement with the experimental findings.

Data availability

All data generated or analyzed during this study are included in this published article and its supplementary information files.

Received: 1 February 2023; Accepted: 31 May 2023

Published online: 03 June 2023

References

- Söylev, T. A. & Richardson, M. G. Corrosion inhibitors for steel in concrete: State-of-the-art report. *Constr. Build. Mater.* **22**, 609. <https://doi.org/10.1016/j.conbuildmat.2006.10.013> (2008).
- Pradhan, B. & Bhattacharjee, B. Rebar corrosion in chloride environment. *Constr. Build. Mater.* **25**, 2565. <https://doi.org/10.1016/j.conbuildmat.2010.11.099> (2011).
- Saraswathy, V. & Song, H.-W. Improving the durability of concrete by using inhibitors. *Build. Environ.* **42**, 464. <https://doi.org/10.1016/j.buildenv.2005.08.003> (2007).
- El-Hacha, R., Mirmiran, A., Cook, A. & Rizkalla, S. Effectiveness of surface-applied corrosion inhibitors for concrete bridges. *J. Mater. Civ. Eng.* **23**, 271. [https://doi.org/10.1061/\(asce\)mt.1943-5533.0000163](https://doi.org/10.1061/(asce)mt.1943-5533.0000163) (2011).
- Harilal, M. *et al.* The chloride-induced corrosion of a fly ash concrete with nanoparticles and corrosion inhibitor. *Constr. Build. Mater.* **274**, 122097. <https://doi.org/10.1016/j.conbuildmat.2020.122097> (2021).
- Chen, Z. & Ye, H. Sequestration and release of nitrite and nitrate in alkali-activated slag: A route toward smart corrosion control. *Cem. Concr. Res.* **143**, 106398. <https://doi.org/10.1016/j.cemconres.2021.106398> (2021).
- Bolzoni, F., Brenna, A. & Ormellese, M. Recent advances in the use of inhibitors to prevent chloride-induced corrosion in reinforced concrete. *Cem. Concr. Res.* **154**, 106719. <https://doi.org/10.1016/j.cemconres.2022.106719> (2022).
- Gaidis, J. M. Chemistry of corrosion inhibitors. *Cem. Concr. Compos.* **26**, 181. [https://doi.org/10.1016/s0958-9465\(03\)00037-4](https://doi.org/10.1016/s0958-9465(03)00037-4) (2004).
- Fouda, A. S., Elewady, G. Y., Shalabi, K. & Abd El-Aziz, H. K. Alcamines as corrosion inhibitors for reinforced steel and their effect on cement-based materials and mortar performance. *RSC Adv.* **5**, 36957. <https://doi.org/10.1039/c5ra00717h> (2015).
- Al-Masoud, M. A. *et al.* Advanced protective films based on binary ZnO-NiO@polyaniline nanocomposite for acidic chloride steel corrosion: An integrated study of theoretical and practical investigations. *Polymers* **14**, 4734. <https://doi.org/10.3390/polym14214734> (2022).
- Kanwal, M., Khushnood, R. A., Shahid, M. & Wattoo, A. G. An integrated and eco-friendly approach for corrosion inhibition and microstructural densification of reinforced concrete by immobilizing *Bacillus subtilis* in pyrolytic sugarcane-bagasse. *J. Clean. Prod.* **355**, 131785. <https://doi.org/10.1016/j.jclepro.2022.131785> (2022).
- Shehnaazdeep, B. Pradhan, A study on effectiveness of inorganic and organic corrosion inhibitors on rebar corrosion in concrete: A review. *Mater. Today Proc.* <https://doi.org/10.1016/j.matpr.2022.04.296> (2022).
- Abd El-Lateef, H. M., Shaaban, S., Khalaf, M. M., Toghian, A. & Shalabi, K. Synthesis, experimental, and computational studies of water soluble anthranilic organoselenium compounds as safe corrosion inhibitors for J55 pipeline steel in acidic oilfield formation water. *Colloids Surf. A Physicochem. Eng. Asp.* **625**, 1268. <https://doi.org/10.1016/j.colsurfa.2021.126894> (2021).
- Eid, A. M., Shaaban, S. & Shalabi, K. Tetrazole-based organoselenium bi-functionalized corrosion inhibitors during oil well acidizing: Experimental, computational studies, and SRB bioassay. *J. Mol. Liq.* **298**, 111980. <https://doi.org/10.1016/j.molliq.2019.111980> (2020).
- Abd El-Lateef, H. M., Sayed, A. R. & Shalabi, K. Synthesis and theoretical studies of novel conjugated polyazomethines and their application as efficient inhibitors for C1018 steel pickling corrosion behavior. *Surf. Interfaces* **23**, 101037. <https://doi.org/10.1016/j.surfint.2021.101037> (2021).

16. Azeredo, J. B. *et al.* “Green is the color”: An update on ecofriendly aspects of organoselenium chemistry. *Molecules* **27**, 1597 (2022).
17. Shaaban, S., El-Lateef, H. M. A., Khalaf, M. M., Gouda, M. & Youssef, I. One-pot multicomponent polymerization, metal-, and non-metal-catalyzed synthesis of organoselenium compounds. *Polymers* **14**, 2208 (2022).
18. Chuai, H. *et al.* Small molecule selenium-containing compounds: Recent development and therapeutic applications. *Eur. J. Med. Chem.* **223**, 113621. <https://doi.org/10.1016/j.ejmech.2021.113621> (2021).
19. Abd El-Lateef, H. M. *et al.* Novel water-soluble organoselenocyanates and symmetrical diselenides tethered N-succinylate and N-maleinylate as corrosion inhibitors for reinforced steel in the simulated concrete pore solution. *Constr. Build. Mater.* **366**, 130135 (2023).
20. Abd El-Lateef, H. M., Shaaban, S., Shalabi, K. & Khalaf, M. M. Novel organoselenium-based N-maleinylate acids as efficacious corrosion inhibitors for 6061 aluminum alloy in molar HCl: In-silico modeling, electrochemical, and surface morphology studies. *J. Taiwan Inst. Chem. Eng.* **133**, 104258 (2022).
21. Abd El-Lateef, H. M., Shaaban, S., Khalaf, M. M., Toghian, A. & Shalabi, K. Synthesis, experimental, and computational studies of water-soluble anthranilic organoselenium compounds as safe corrosion inhibitors for J55 pipeline steel in acidic oilfield formation water. *Colloids Surf. A* **625**, 126894 (2021).
22. Eid, A. M., Shaaban, S. & Shalabi, K. Tetrazole-based organoselenium bi-functionalized corrosion inhibitors during oil well acidizing: Experimental, computational studies, and SRB bioassay. *J. Mol. Liq.* **298**, 111980 (2020).
23. Shaaban, S., Ashmawy, A. M., Negm, A. & Wessjohann, L. A. Synthesis and biochemical studies of novel organic selenides with increased selectivity for hepatocellular carcinoma and breast adenocarcinoma. *Eur. J. Med. Chem.* **179**, 515. <https://doi.org/10.1016/j.ejmech.2019.06.075> (2019).
24. Shaaban, S., Negm, A., Ashmawy, A. M., Ahmed, D. M. & Wessjohann, L. A. Combinatorial synthesis, in silico, molecular and biochemical studies of tetrazole-derived organic selenides with increased selectivity against hepatocellular carcinoma. *Eur. J. Med. Chem.* **122**, 55. <https://doi.org/10.1016/j.ejmech.2016.06.005> (2016).
25. Shaaban, S., Arafat, M. A., Gaffer, H. E. & Hamama, W. S. Synthesis and anti-tumor evaluation of novel organoselenocyanates and symmetrical diselenides dyestuffs. *Der Pharma Chemica* **6**, 186 (2014).
26. Shaaban, S. *et al.* Cytoprotective organoselenium compounds for oligodendrocytes. *Arab. J. Chem.* **14**, 103051 (2021).
27. El-Senduny, F. F. *et al.* Urea-functionalized organoselenium compounds as promising anti-HepG2 and apoptosis-inducing agents. *Future Med. Chem.* **13**, 1655 (2021).
28. Shaaban, S., Shabana, S. M., Al-Faiyz, Y. S., Manolikakes, G. & El-Senduny, F. F. Enhancing the chemosensitivity of HepG2 cells towards cisplatin by organoselenium pseudopeptides. *Bioorg. Chem.* **109**, 1047. <https://doi.org/10.1016/j.bioorg.2021.104713> (2021).
29. Fang, X.-L., Tang, R.-Y., Zhang, X.-G. & Li, J.-H. FeF₃/I₂-catalyzed synthesis of 4-chalcogen-substituted arylamines by direct thiolation of an arene CH bond. *Synthesis* **2011**, 1099 (2011).
30. Xueyuan, W. & Asok, K. R. Density-functional study of water adsorption on the PuO₂(110) surface. *Phys. Rev. B* **65**, 85403 (2002).
31. Modelling and Simulation Solutions for Chemicals and Materials Research, Materials Studio (Version 5.0), Accelrys Software Inc., San Diego, USA. Available online at: www.accelrys.com (2009).
32. Yousef, T. A., Abu El-Reash, G. M., El-Gamal, O. & Sharaa, B. M. Ligational, DFT, optical band gap and biological studies on Mn(II), Co(II) and Ni(II) complexes of ethyl and allyl thiosemicarbazides ending by thiazole group. *J. Mol. Liq.* **251**, 423 (2018).
33. Youssef, H. M., Abdulhamed, Y. K., Abu El-Reash, G. M. & Yousef, T. A. Cr(III) and Ni(II) complexes of isatin-hydrazone ligand: Preparation, characterization, DFT studies, biological activity, and ion-flotation separation of Ni(II). *Inorg. Chem. Commun.* **138**, 1092 (2022).
34. Yousef, T. A., Alduaij, O. K., Ahmed, S. F., Abu El-Reash, G. M. & El-Gammal, O. A. Structural, DFT and biological studies on Cr(III) complexes of semi and thiosemicarbazide ligands derived from diketo hydrazide. *J. Mol. Struct.* **1125**, 788 (2016).
35. Yousef, T. A., Alduaij, O. K., Ahmed, S. F., Abu El-Reash, G. M. & El-Gammal, O. A. Semi- and thiosemicarbazide Mn(II) complexes: Characterization, DFT and biological studies. *J. Mol. Struct.* **1119**, 351 (2016).
36. Kaya, S. *et al.* Quantum chemical and molecular dynamic simulation studies for the prediction of inhibition efficiencies of some piperidine derivatives on the corrosion of iron. *J. Taiwan Inst. Chem. Eng.* **65**, 522 (2016).
37. Yousef, T. A. *et al.* Environment-friendly corrosion inhibitors for aluminum in hydrochloric acid: Quantum and experimental research. *Metals* **12**, 1538. <https://doi.org/10.3390/met12091538> (2022).
38. Abd El-Lateef, H. M., Shalabi, K. & Tantawy, A. H. Corrosion inhibition and adsorption features of novel bioactive cationic surfactants bearing benzenesulphonamide on C1018-steel under sweet conditions: Combined modeling and experimental approaches. *J. Mol. Liq.* **320**, 114564. <https://doi.org/10.1016/j.molliq.2020.114564> (2020).
39. Chahmout, H. *et al.* New pyrazole compounds as a corrosion inhibitor of stainless steel in 2.0 M H₂SO₄ medium: Electrochemical and theoretical insights. *Inorg. Chem. Commun.* **147**, 110150. <https://doi.org/10.1016/j.inoche.2022.110150> (2023).
40. Rbaa, M. *et al.* Synthesis of new halogenated compounds based on 8-hydroxyquinoline derivatives for the inhibition of acid corrosion: Theoretical and experimental investigations. *Mater. Today Commun.* **33**, 104654. <https://doi.org/10.1016/j.mtcomm.2022.104654> (2022).
41. Abouchane, M. *et al.* Insight into the corrosion inhibition performance of two quinoline-3-carboxylate derivatives as highly efficient inhibitors for mild steel in acidic medium: Experimental and theoretical evaluations. *J. Mol. Liq.* **360**, 119470. <https://doi.org/10.1016/j.molliq.2022.119470> (2022).
42. Al Kiey, S. A., Hasanin, M. S. & El-Taib, H. F. Green and sustainable chitosan-gum Arabic nanocomposites as efficient anticorrosive coatings for mild steel in saline media. *Sci. Rep.* **12**(1), 13209. <https://doi.org/10.1038/s41598-022-17386-7> (2022).
43. Oubaaqa, M. *et al.* Experimental and theoretical investigation of corrosion inhibition effect of two 8-hydroxyquinoline carbonitrile derivatives on mild steel in 1 M HCl solution. *J. Phys. Chem. Solids* **169**, 110866. <https://doi.org/10.1016/j.jpcc.2022.110866> (2022).
44. Mansfeld, F. Electrochemical impedance spectroscopy (EIS) as a new tool for investigating methods of corrosion protection. *Electrochim. Acta.* **35**, 1533. [https://doi.org/10.1016/0013-4686\(90\)80007-b](https://doi.org/10.1016/0013-4686(90)80007-b) (1990).
45. Flis, J. & Zakroczyński, T. Impedance study of reinforcing steel in simulated pore solution with Tannin. *J. Electrochem. Soc.* **143**, 2458. <https://doi.org/10.1149/1.1837031> (1996).
46. Ech-chebab, A. *et al.* Evaluation of quinoxaline-2(1H)-one, derivatives as corrosion inhibitors for mild steel in 1.0 M acidic media: Electrochemistry, quantum calculations, dynamic simulations, and surface analysis. *Chem. Phys. Lett.* **809**, 140156. <https://doi.org/10.1016/j.cplett.2022.140156> (2022).
47. Abdallah, Y. M., Shalabi, K. & Bayoumy, N. M. Eco-friendly synthesis, biological activity and evaluation of some new pyridopyrimidinone derivatives as corrosion inhibitors for API 5L X52 carbon steel in 5% sulfamic acid medium. *J. Mol. Struct.* **1171**, 658. <https://doi.org/10.1016/j.molstruc.2018.06.045> (2018).
48. El Badry, M. M. & El-Taib, H. F. Potential application of carbon-based/ionophore electrical sensor for the highly sensitive diltiazem HCl quantification in its pharmaceutical products and biological samples. *Electroanalysis* **34**, 1. <https://doi.org/10.1002/elan.20220041> (2022).
49. Salasi, M., Shahrabi, T., Roayaei, E. & Aliofkhaeaei, M. The electrochemical behavior of environment-friendly inhibitors of silicate and phosphonate in corrosion control of carbon steel in soft water media. *Mater. Chem. Phys.* **104**, 183. <https://doi.org/10.1016/j.matchemphys.2007.03.008> (2007).

50. Abdel-Rehim, S. S., Khaled, K. F. & Abd-Elshafi, N. S. Electrochemical frequency modulation as a new technique for monitoring corrosion inhibition of iron in acid media by new thiourea derivative. *Electrochim. Acta.* **51**, 3269. <https://doi.org/10.1016/j.electacta.2005.09.018> (2006).
51. Abd El-Lateef, H. M., Alnajjar, A. O. & Khalaf, M. M. Advanced self-healing coatings based on ZnO, TiO₂, and ZnO-TiO₂/polyvinyl chloride nanocomposite systems for corrosion protection of carbon steel in acidic solutions containing chloride. *J. Taiwan Inst. Chem. Eng.* **116**, 286. <https://doi.org/10.1016/j.jtice.2020.11.015> (2020).
52. Abd El-Lateef, H. M. & Khalaf, M. M. Fabrication and characterization of alumina-silica/poly(o-toluidine) nanocomposites as novel anticorrosive epoxy coatings films on carbon steel. *Microchem. J.* **158**, 105129. <https://doi.org/10.1016/j.microc.2020.105129> (2020).
53. Hussein, R. K., Abou-Krishna, M. & Yousef, T. A. Theoretical and experimental studies of different amine compounds as corrosion inhibitors for aluminum in hydrochloric acid. *Biointerface Res. Appl. Chem.* **11**(2), 9772. <https://doi.org/10.33263/BRIAC112.97729785> (2021).
54. Ouakki, M. *et al.* Detailed experimental and computational explorations of pyran derivatives as corrosion inhibitors for mild steel in 1.0 M HCl: Electrochemical/surface studies, DFT modeling, and MC simulation. *J. Mol. Struct.* **1261**, 132784. <https://doi.org/10.1016/j.molstruc.2022.132784> (2022).
55. Paliappan, N., Cole, I. S. & Kuznetsov, A. E. Experimental and computational studies of graphene oxide covalently functionalized by octylamine: Electrochemical stability, hydrogen evolution, and corrosion inhibition of the AZ13 Mg alloy in 3.5% NaCl. *RSC Adv.* **10**, 11426. <https://doi.org/10.1039/c9ra10702a> (2020).
56. Gao, G. & Liang, C. Electrochemical and DFT studies of β -amino-alcohols as corrosion inhibitors for brass. *Electrochim. Acta.* **52**, 4554. <https://doi.org/10.1016/j.electacta.2006.12.058> (2007).
57. Abd El-Lateef, H. M., Shalabi, K. & Tantawy, A. H. Corrosion inhibition of carbon steel in hydrochloric acid solution using newly synthesized urea-based cationic fluorosurfactants: Experimental and computational investigations. *New J. Chem.* **44**, 17791. <https://doi.org/10.1039/d0nj04004e> (2020).
58. Goyal, M. *et al.* Acid corrosion inhibition of ferrous and non-ferrous metal by nature friendly Ethoxycarbonylmethyltriphenylphosphonium Bromide (ECMTPB): Experimental and MD simulation evaluation. *J. Mol. Liq.* **315**, 113705. <https://doi.org/10.1016/j.molliq.2020.113705> (2020).
59. Oyebamiji, A. K. & Adeleke, B. B. Quantum chemical studies on inhibition activities of 2,3-dihydroxypropyl-sulfanyl derivative on carbon steel in acidic media. *Int. J. Corros. Scale Inhib.* **7**, 498. <https://doi.org/10.17675/2305-6894-2018-7-4-2> (2018).
60. Hsissou, R. *et al.* Synthesis and anticorrosive properties of epoxy polymer for CS in [1 M] HCl solution: Electrochemical, AFM, DFT and MD simulations. *Constr. Build. Mater.* **270**, 121454. <https://doi.org/10.1016/j.conbuildmat.2020.121454> (2021).
61. Guo, L. *et al.* Anticorrosive effects of some thiophene derivatives against the corrosion of iron: A computational study. *Front. Chem.* **6**, 155. <https://doi.org/10.3389/fchem.2018.00155> (2018).
62. Hsissou, R. Review on epoxy polymers and its composites as a potential anticorrosive coatings for carbon steel in 3.5% NaCl solution: Computational approaches. *J. Mol. Liq.* **336**, 116307. <https://doi.org/10.1016/j.molliq.2021.116307> (2021).
63. Gece, G. & Bilgiç, S. Quantum chemical study of some cyclic nitrogen compounds as corrosion inhibitors of steel in NaCl media. *Corros. Sci.* **51**, 1876. <https://doi.org/10.1016/j.corsci.2009.04.003> (2009).
64. Madkour, L. H., Kaya, S. & Obot, I. B. Computational, Monte Carlo simulation and experimental studies of some arylazotriazoles (AATR) and their copper complexes in corrosion inhibition process. *J. Mol. Liq.* **260**, 351. <https://doi.org/10.1016/j.molliq.2018.01.055> (2018).
65. Shalabi, K., Helmy, A. M., El-Askalany, A. H. & Shahba, M. M. New pyridinium bromide mono-cationic surfactant as corrosion inhibitor for carbon steel during chemical cleaning: Experimental and theoretical studies. *J. Mol. Liq.* **293**, 111480. <https://doi.org/10.1016/j.molliq.2019.111480> (2019).
66. Özcan, M., Dehri, I. & Erbil, M. Organic sulphur-containing compounds as corrosion inhibitors for mild steel in acidic media: Correlation between inhibition efficiency and chemical structure. *Appl. Surf. Sci.* **236**, 155. <https://doi.org/10.1016/j.apsusc.2004.04.017> (2004).
67. Dehghani, A., Mostafatabar, A. H., Bahlakeh, G. & Ramezanzadeh, B. A detailed study on the synergistic corrosion inhibition impact of the Quercetin molecules and trivalent europium salt on mild steel; electrochemical/surface studies, DFT modeling, and MC/MD computer simulation. *J. Mol. Liq.* **316**, 113914. <https://doi.org/10.1016/j.molliq.2020.113914> (2020).

Acknowledgements

The authors acknowledge the Deanship of Scientific Research, Vice Presidency for Graduate Studies and Scientific Research at King Faisal University, Saudi Arabia, for financial support under the annual funding track (GRANT 3503). The authors extend their appreciation to the Deanship of Scientific Research at Imam Mohammed Ibn Saudi Islamic University for funding this work through Research Group No. RG-21-09-80.

Author contributions

H.M.A.E.: Conceptualization, Supervision, Investigation, Methodology, Resources, Formal analysis, Data curation, Funding acquisition, Writing-original draft, Writing-review & editing. M.M.K.: Formal analysis, Data curation, Funding acquisition, Writing-original draft, Writing-review & editing. M.G.: Funding acquisition, Writing-original draft, Writing-review & editing. T.A.Y.: Conceptualization, Investigation, Methodology, Resources, Formal analysis, Data curation, Funding acquisition, Writing-original draft, Writing-review & editing. S.H.K.: Writing-original draft, Writing-review & editing. M.M.A.-K.: Writing-original draft, Writing-review & editing. M.A.: Writing-original draft, Writing-review & editing. S.S.: Conceptualization, Investigation, Methodology, Resources, Formal analysis, Data curation, Funding acquisition, Writing-original draft, Writing-review & editing. All co-authors contributed to data collection, and review and approval of the final manuscript.

Funding

This research was funded by the Deanship of Scientific Research, Saudi Arabia (GRANT3,503).

Competing interests

The authors declare no competing interests.

Additional information

Supplementary Information The online version contains supplementary material available at <https://doi.org/10.1038/s41598-023-36222-0>.

Correspondence and requests for materials should be addressed to H.M.A.-L. or S.S.

Reprints and permissions information is available at www.nature.com/reprints.

Publisher's note Springer Nature remains neutral with regard to jurisdictional claims in published maps and institutional affiliations.



Open Access This article is licensed under a Creative Commons Attribution 4.0 International License, which permits use, sharing, adaptation, distribution and reproduction in any medium or format, as long as you give appropriate credit to the original author(s) and the source, provide a link to the Creative Commons licence, and indicate if changes were made. The images or other third party material in this article are included in the article's Creative Commons licence, unless indicated otherwise in a credit line to the material. If material is not included in the article's Creative Commons licence and your intended use is not permitted by statutory regulation or exceeds the permitted use, you will need to obtain permission directly from the copyright holder. To view a copy of this licence, visit <http://creativecommons.org/licenses/by/4.0/>.

© The Author(s) 2023